Density of ethanolic alkali halide salt solutions by experiment and molecular simulation

Steffen Reiser, Martin Horsch*, Hans Hasse

Laboratory of Engineering Thermodynamics, University of Kaiserslautern
67653 Kaiserslautern, Germany

Abstract

The density of ethanolic electrolyte solutions of all soluble alkali halide salts (LiCl, LiBr, LiI, NaBr, NaI, and KI) is studied at 298.15, 308.15, 318.15, and 328.15 K at concentrations up to 0.05 mol/mol or 90 % of the solubility limit both by experiment and molecular simulation. The force fields used for describing the ions are of the Lennard-Jones (LJ) plus point charge type, the ethanol force field is of the LJ plus partial charges type. All force fields were taken from previous work of our group and where adjusted to properties of aqueous solutions in case of the ions [J. Chem. Phys. **136**, 084501 (2012), J. Chem. Phys. **140**, 044504 (2014)] and to pure component properties [Fluid Phase Equilib. **236**, 272 (2005)] in case of the solvent. The Lorentz-Berthelot combining rule is used to determine the mixed interactions between ions and ethanol. The present simulations are hence predictions as no parameters are adjusted to properties of ethanolic electrolyte solutions. The predictions of the reduced density are found to be in good agreement with the experimental data. Furthermore, the radial distribution function of the ethanol sites around the ions, the solvation number and the residence

*Corresponding author
Email address: martin.horsch@mv.uni-kl.de (Martin Horsch)

time of ethanol molecules in the first solvation shell, the self-diffusion coefficient of the ions and the electric conductivity are systematically studied by molecular simulation and compared to experimental data where available.

Keywords: ethanolic electrolyte solutions, alkali halide salts, density measurements, molecular simulation

1. Introduction

In the last decades, organic electrolyte solutions have become increasingly important in many industrial applications, especially in the field of electrochemistry [1, 2]. The investigation of the thermodynamic properties of organic electrolyte solutions is therefore of particular interest [3].

We recently published a comprehensive molecular simulation study of thermodynamic properties of methanolic alkali halide salt solutions [4] with classical force fields, which were taken from previous work of our group. The ion force fields had been adjusted to properties of aqueous alkali halide salt solutions [5, 6] and the solvent methanol to pure component properties [7]. No parameters were adjusted to properties of methanolic electrolyte solutions. The predictions of the reduced density, i.e. the density of the electrolyte solution divided by the density of the pure solvent at the same temperature, were found to be in very good agreement with experimental data over a wide temperature and concentration range [4]. The same holds for other studied properties which include: the first maximum in the radial distribution function (RDF) of the hydroxyl and the methyl group of the methanol molecule around the ions, the solvation number, the self-diffusion coefficient of the ion in the solution, and the electric conductivity. Such good agreement could not be expected a priori. To see whether the encouraging findings for

2

the methanolic electrolyte solution were just a lucky coincidence or whether our approach is capable of predicting thermodynamic properties of organic electrolyte solutions more generally, the present study extends the previous work to ethanolic alkali halide salt solutions. The methodology is largely unchanged and therefore only briefly described here.

The main focus was again on the reduced density of the electrolyte solutions. As there is a lack of experimental density data in the literature, the density of ethanolic electrolyte solutions of all soluble alkali halide salts (LiCl, LiBr, LiI, NaBr, NaI and KI) was studied systematically not only by molecular simulation but also by experiments at temperatures between 298.15 and 328.15 K and salt concentrations up to 0.05 mol/mol or 90 % of the solubility limit. At 298.15 K, there is literature data in that concentration range for LiCl [8, 9, 10, 11, 12], NaBr [9, 12], NaI [13, 9, 14, 15, 10, 16, 12], and KI [9] but not for LiBr [10, 12] and LiI [10, 12] solutions. At the other investigated temperatures, namely 308.15, 318.15 and 328.15 K, experimental density data of ethanolic alkali halide salt solutions was up to now entirely missing in the literature. The molecular simulations were carried out for the same temperature and composition as studied in the experiments of the present work.

In the literature, there are only a few simulation studies on the thermodynamic properties of ethanolic alkali halide salt solutions [17, 12, 18, 19]. Held et al. [12] modeled the liquid densities, the osmotic coefficient, and the mean ionic activity coefficients of ethanolic electrolyte solutions with the ePC-Saft equation of state and validated the results against own measurements. Zeng and co-workers [18, 19] investigated the structure of the solvent around Li^+ and Na^+ and dynamic properties like the auto-correlation function of these ions in ethanolic solutions by

3

Car-Parrinello molecular dynamics simulations. Yan et al. [17] used molecular simulations with classical force fields to study osmotic effects in ethanolic NaBr salt solutions with a membrane type simulation method [17]. The force field for ethanol was taken from Jorgensen [20], that for the ions (Na^+ and Br^-) from Jorgensen et al. [21]. A geometric mixing rule was used and no interaction parameters were adjusted [17]. To the best of our knowledge, no other reports on molecular simulation with classical force fields of thermodynamic properties of ethanolic alkali halide salt solutions are available in the literature.

Several ethanol force fields are available in the literature [20, 22, 23, 24, 25]. From these, we have chosen one developed previously in our group by Schnabel et al. [25] which is known to give good results both for thermodynamic properties of pure ethanol and ethanol-containing non-ionic mixtures [25, 26, 27, 28, 29]. The parameters of the ethanol model were adjusted to the vapor-liquid equilibrium of pure ethanol [25], namely the saturated liquid density and the vapor pressure. The temperature dependence of the density of pure liquid ethanol at 1 bar is shown in Figure 1. The density of pure ethanol is slightly overestimated by the model over the entire investigated temperature range. The highest deviation from experimental data of about 0.6 % is found at 298.15 K. With increasing temperature, the deviations decrease.

The force fields used for the ions [5, 6] were taken from previous work of our group. Their parameters were adjusted with SPC/E water [31] to properties of aqueous electrolyte solutions, namely the reduced density, the self-diffusion coefficient of the ions in the solution and the first maximum in the RDF of water around the ions at 293.15 and 298.15 K, respectively, and 1 bar [5, 6]. They describe many thermodynamic properties of aqueous alkali halide solutions well,

4

also outside the range they were adjusted to [5, 6, 32]. As in our study on methanolic electrolyte solutions [32], Lorentz-Berthelot combining rules were used to determine the mixed interactions between ions and solvent and no parameters were adjusted to the properties of ethanolic alkali halide salt solutions so that all simulations results presented here are predictions.

A focus of the present study was to evaluate predictions for the reduced density of the solution which is defined as

$$\widetilde{\rho} = \frac{\rho}{\rho_{\mathrm{EtOH}}} \; ,\tag{1}$$

where ρ_{EtOH} is the density of pure ethanol at the same temperature and pressure as the density of the solution ρ. It is used as reference property to minimize the influence of the error in the ethanol model on the simulation results, cf. Figure 1. For the calculation of the reduced density, the density of pure ethanol has to be known. In the case of experimental data, it is taken from the present measurements of pure ethanol, in the case of simulation results, it is determined in present pure ethanol simulations.

Besides the reduced density also, structural, dynamic, and transport properties of ethanolic alkali halide salt solutions were systematically studied in the present work by molecular simulation at 298.15 K and compared to experimental literature data where available.

Throughout this study all properties were investigated at 1 bar and the composition is given in terms of the ion mole fraction x_i, which is defined as

$$x_i = \frac{n_i}{2 \cdot n_i + n_{\mathrm{EtOH}}} \; ,\tag{2}$$

5

where n_i is the mole number of each ion type and n_{EtOH} the mole number of ethanol molecules in the electrolyte solution. For the 1:1 salt studied here, the ion mole fraction of the anions and the cations is x_i each. Some other studies quantify the salinity in terms of the overall salt mole fraction, regarding the salt as a single component. The ion mole fraction x_i is related to the overall salt mole fraction x_{S}

$$x_{\mathrm{S}} = \frac{n_{\mathrm{S}}}{n_{\mathrm{S}} + n_{\mathrm{W}}} \tag{3}$$

by

$$x_{\mathrm{S}} = \frac{x_i}{1 - x_i} \tag{4}$$

as the mole number of salt in the solution is $n_{\mathrm{S}} = n_i$ here.

In Section 2 of the present paper, the experiments are described. The employed force fields and the simulation methods are introduced in Section 3. In Section 4, the experimental data and the simulation results are presented and discussed. Section 5 summarizes the main statement from the present work.

2. Experiments

For the preparation of the ethanolic alkali halide salt solutions pure ethanol ($\geq$99.9 %, ROTISOLV Roth) was used. The purity and the supplier of the alkali halide salts are shown in Table 1. The treatment of the salts, the preparation of the samples of electrolyte solutions and the density measurements are identical to the procedures described in detail in recent work [4]. The uncertainty of the concentration x_i is estimated by error propagation considering the resolution of the balance and the error by determining the concentrations gravimetrically to be for all samples below ± 0.00001 mol/mol. Based on the resolution of the densimeter and results from

the repetition of experiments at the same conditions, the uncertainty of the density measurements was found to be better than ±0.0001 g/cm³. The uncertainty of the temperature measurements is better than ±0.1 K. In the literature, several publications of the solubility limit of alkali halide salts in ethanol are available [33, 34, 35, 36, 37, 38, 39, 40, 41, 42, 43, 44, 45, 46, 47, 48, 49, 50, 51, 52, 53]. The analysis of these data reveals that most alkali halide salts are only soluble in traces in ethanol. However, the solubility limit of LiCl [52], LiBr [40], LiI [34], NaBr [41], NaI [41] and KI [41] is high enough to cover a reasonable concentration range both for the experiments and the molecular simulations.

3. Molecular simulation

In this study, rigid, non-polarizable force fields of the LJ (ions) and united-atom LJ (EtOH) type with superimposed point charges were used. The force fields for ethanol [25] and the alkali cations and halide anions [5, 6] were taken from previous work of our group. The ethanol model consists of three united-atom LJ sites which account for repulsion and dispersion of the methylene, methyl and hydroxyl group. To model both polarity and hydrogen bonding, the ethanol model additionally possesses three point charges which are located at the center of the methylene group and the position of the oxygen and hydrogen atom of the hydroxyl group. Figure 2 shows the geometry of the ethanol force field and its parameters are listed in Table 2. The ion force fields consist of one LJ site and a concentric point charge with the magnitude of ±1 e. Their LJ parameters are specified in Table 3. For the unlike LJ parameters of all interactions, i.e. ion-solvent and ion-ion (different types), the Lorentz-Berthelot [54, 55] combining rules were used.

In the present study, the reduced density of the solutions, the radial distribution

function of the hydroxyl $g_{i-\mathrm{O}}(r)$, the methylene $g_{i-\mathrm{CH2}}(r)$ and the methyl group $g_{i-\mathrm{CH3}}(r)$ of ethanol around the ion i, the solvation number $n_{i-\mathrm{O}}$ and the residence time $\tau_{i-\mathrm{O}}$ of ethanol molecules in the first solvation shell around the ion, the self-diffusion coefficient D_i of the ions, and the electric conductivity σ of the solutions were determined by molecular simulation at 298.15 K. The methods for the calculation of these properties are described in detail in previous work [4]. For the determination of $g_{i-\mathrm{O}}(r)$ the position of the hydroxyl group and for $n_{i-\mathrm{O}}$ and $\tau_{i-\mathrm{O}}$ the position of the ethanol molecule is represented by the position of the oxygen atom. All properties of ethanolic electrolyte solutions were determined at low salinity (except the reduced density), and hence their simulation results are almost independent on the counterion in the solution.

Following a proposal by Impey et al. [56], unpairing of an ion and an ethanol molecule was defined to occur if their separation lasted longer than the average residence time $\tau_{\mathrm{O-O}}$ of an ethanol molecule around a neighboring molecule in a pure bulk ethanol simulation at the same conditions. However, a short-time pairing of two particles $\tau_{i-\mathrm{O}} < \tau_{\mathrm{O-O}}$ was fully accounted for in the calculation $\tau_{i-\mathrm{O}}$. The simulation program $ms2$ [57] was used for all simulations carried out in the present work. Technical details are given in the Appendix.

4. Results and discussion

4.1. Experimental density data

The experimental density data for ethanolic electrolyte solutions of all soluble alkali halide salts as well as for pure liquid ethanol are presented in Table 4. In Figure 3, the present experimental density data of ethanolic electrolyte solutions are compared to literature data [8, 9, 10, 11, 12, 13, 14, 15, 16] at 298.15 K over

8

the entire investigated concentration range. The deviations from the literature data are generally below 0.1 %, for the LiBr and KI salt solutions even below 0.05 %. For one data point of Held et al. [12] for LiCl salt solutions at high concentration the deviation is slightly above 0.1 %. However, the deviations from the data of Vosburgh et al. [8] in the same regime are below 0.1 %, cf. Figure 3. The deviation from the data of Partington and Simpson [13] in case of NaI is 1.1 % at the highest concentration measured by these authors, apart from that it is below 0.05 %. According to Figure 3, there is also a mismatch between this data point of Partington and Simpson [13] and the remaining literature data [14, 15, 10, 12]. Figure 3 and Table 4 reveal that the density ρ increases linearly with increasing ion mole fraction x_i at a given temperature for all investigated ethanolic alkali halide salt solutions:

$$\rho(x_i, T) = \rho_{\text{EtOH}}(T) + a(T) \cdot x_i \,. \tag{5}$$

The numbers for the slopes a at 298.15 and 328.15 K obtained for each salt from a linear fit to the experimental data of the present work are given in Table 5. The standard deviation of the linear correlation of the density according to Eq. (5), is below ± 0.001 g/cm^3 for all studied solutions. As can be seen from Table 5, the slopes a depend on the salt but are almost independent on the temperature. Hence, the temperature dependence of the density of the studied ethanolic alkali halide salt solutions is determined only by the temperature dependence of the density of pure ethanol. In Figure 4, the temperature dependence of the density of pure ethanol and of the different investigated NaI salt solutions is shown as an example. The reduced density $\widetilde{\rho}$ of the electrolyte solutions is therefore almost independent on the temperature as well.

9

4.2. Comparison of simulation results and experimental density data

The simulation results for the density ρ of the investigated ethanolic alkali halide salt solutions and of pure liquid ethanol are given in Table 6.

In Figure 5, the predictions from molecular simulation for the reduced density $\widetilde{\rho}$ of the studied electrolyte solutions are compared to the present experimental data at 298.15 and 328.15 K. At 298.15 K, an fair agreement between simulation results and experimental data is found in case of the lithium halide (LiCl, LiBr and LiI) salt solutions. The deviations increase up to 1.7 % at the highest investigated concentration. In case of the remaining alkali halide salt (NaBr, NaI, KI) solutions, a good agreement with deviations below 0.5 % between simulation results and experimental data is found over the entire investigated concentration range, cf. Figure 5. The experimental data of $\widetilde{\rho}$ are found to be almost temperature-independent, which is well predicted by the simulation results, cf. Figure 5.

At a given temperature, the simulation results of the density ρ of all investigated ethanolic electrolyte solutions increase linearly with increasing ion mole fraction x_i, cf. Eq. 5. In Figure 6, the slopes a of the ethanolic electrolyte solution density, determined from the present experimental data, are compared to simulation results at 298.15 and 328.15 K. The predictions of a from molecular simulation are found to be almost temperature-independent, which is consistent with the experimental data, cf. Figure 6. The slope a increases in general with increasing size both of the cations and the anions, but that effect is more important for the anions than it is for the cations. This is a consequence of the different arrangement of the ethanol molecules in the solvation shell around the oppositely charged ions, cf. discussion below.

10

4.3. Structural properties

The RDF of ethanol around the alkali cations (Li$^+$, Na$^+$, and K$^+$) and halide anions (Cl$^-$, Br$^-$, and I$^-$) in ethanolic solutions was determined for the oxygen atom $g_{i-O}(r)$, the methylene $g_{i-CH2}(r)$ and the methyl group $g_{i-CH3}(r)$ by molecular simulation at 298.15 K and low salinity (x_i= 0.002 mol/mol) in LiCl, NaBr and KI salt solutions.

The simulation results for the extrema of the RDF are listed in Table 7. As an example, the RDF of the ethanol sites around the sodium cation and the chloride anion are shown in Figure 7. As expected, the position of the first maximum $r_{\text{max},1}$ of $g_{i-O}(r)$ is for both cations and anions closer to the ion than $r_{\text{max},1}$ of $g_{i-CH2}(r)$ and $g_{i-CH3}(r)$, respectively (cf. Figure 7 and Table 7). The hydroxyl group of the ethanol molecules points towards the ion and the methylene and methyl group generally face into the opposite direction. The position of the first maximum in the RDF of the oxygen atom around the ions is identical to the $r_{\text{max},1}$ data of $g_{i-O}(r)$ in aqueous alkali halide salt solutions with SPC/E water [31] from previous work [6]. This was also observed by Zeng and co-workers [18, 19] in their simulation studies of Li$^+$ and Na$^+$ in aqueous and ethanolic solutions. Furthermore, the present $r_{\text{max},1}$ data of $g_{i-O}(r)$ are identical to the corresponding simulation results in methanolic electrolyte solutions determined in recent work [4]. The density is highly affected by the microscopic structure in the electrolyte solutions. The primary effect on this structure is the distance between the ion and the nearest site of the solvent molecules, which is identical in aqueous, methanolic and ethanolic alkali halide salt solutions. The secondary effect is the orientation of the solvent molecules in the solvation shell around the ions, which is apparently well predicted in the present molecular simulations of ethanolic electrolyte solutions.

11

The simulation results of the position of the first maximum of $g_{i-\mathrm{O}}(r)$, $g_{i-\mathrm{CH2}}(r)$ and $g_{i-\mathrm{CH3}}(r)$ are compared to each other in Figure 8. The LJ size parameters of the lithium and sodium cation are almost identical ($\sigma_{\mathrm{Li}} = 1.88$ Å, $\sigma_{\mathrm{Na}} = 1.89$ Å) and hence the positions $r_{\mathrm{max,1}}$ in the RDF of the oxygen atom, the methylene and the methyl group of ethanol around the two cations are found to be the same within their statistical uncertainties. According to Figure 8, the position of the first maximum increases for $g_{i-\mathrm{O}}(r)$, $g_{i-\mathrm{CH2}}(r)$ and $g_{i-\mathrm{CH3}}(r)$ with increasing size of the ions. In case of the anions a linear increase can be observed with identical slopes for the RDF of the different sites.

Especially remarkable is the change in the order of the first maxima of the methylene and the methyl group around the cations and anions, cf. Figure 8. While the methyl group of the ethanol molecule is closer to the cations than the methylene group, this order is found to be obverse around the anions, cf. Figures 7 and 8. Furthermore, the distance between the $r_{\mathrm{max,1}}$ data of $g_{i-\mathrm{CH3}}(r)$ and $g_{i-\mathrm{CH2}}(r)$ is significantly larger around the anions than around the cations. Both effects can be attributed to the angled shape of the ethanol molecule (cf. Figure 2) and the different orientation of the hydroxyl group around the oppositely charged ions. For illustration purposes, the typical orientation of the ethanol molecules around a cation and anion, respectively, is shown in Figure 9. In case of the cations, the negatively charged hydrogen atom of the hydroxyl group and, in case of the anions, the positively charged oxygen atom points towards the ion, cf. Figure 9. The particular behaviour of $r_{\mathrm{max,1}}$ is additionally increased by the electrostatic repulsion of the positively charged methylene group around cations and its attraction around anions, respectively.

4.4. Solvation number

The solvation number n_{i-O} of ethanol molecules in the first solvation shell around the alkali cations and halide anions was determined at 298.15 K. The calculation of n_{i-O} is based on the RDF $g_{i-O}(r)$ from Section 4.3.

The simulation results of n_{i-O} around the different ions in ethanolic solutions are shown in Figure 10 and listed in Table 8. In case of the alkali cations, an increase of the solvation number with increasing ion size is found as a bigger ion surface provides more space for the attachment of the ethanol molecules. However, around the alkali anions n_{i-O} slightly decreases with the size of the ions from Cl$^-$ to I$^-$, cf. Figure 10 and Table 8. In this case, the influence of the bigger ion surface on n_{i-O} is suppressed by the effect, that with increasing ion size the electrostatic attraction of the ion on the solvent molecule decreases. Hence, an attachment of ethanol molecules in the solvation shell around the ions is less likely to occur. This behaviour was also observed in electrolyte solutions with a different alcoholic solvent, i.e. in systematic simulation studies of the solvation number in methanolic alkali halide salt solutions published by Chowdhuri and Chandra [58] and by Reiser et al. [4]. The present results are in very good agreement with the simulation data for $n_{\mathrm{Li-O}}$ and $n_{\mathrm{Na-O}}$ in ethanolic electrolyte solutions published by Zeng and co-workers [18, 19].

4.5. Solvation dynamics

The residence time τ_{i-O} of ethanol molecules in the first solvation shell around the alkali cations and halide anions was determined at 298.15 K by MD simulation. The simulation results of τ_{i-O} were determined under the same conditions in the same ethanolic electrolyte solutions as the RDF in Section 4.3.

The residence time $\tau_{\mathrm{O-O}}$ of an ethanol molecule around a neighboring molecule

13

in pure liquid ethanol was determined by MD simulation at the same conditions and was found to be τ_{O-O}= 2.4 ps. This time span was set to the period of short time unpairing, which is fully accounted to the calculation of τ_{i-O} during the simulation (cf. Section 3).

The simulation results of the residence time τ_{i-O} of ethanol around the different ions are listed in Table 8. Around the alkali cations, a substantial decrease of the residence time with increasing size of the ions is observed, cf. Table 8. With increasing size, the electrostatic interaction between the ion and the solvent molecules decreases and hence the ethanol molecules are more likely to leave the first solvation shell around the ions. In case of the halide anions, the electrostatic attraction between ions and ethanol molecules in the solvation shell is weak in comparison to the significant smaller alkali cations. Hence, the observed residence time τ_{i-O} of ethanol molecules around the halide anions is only slightly above the residence time τ_{O-O} in pure liquid ethanol.

4.6. Self-diffusion coefficient

The self-diffusion coefficient D_i of the alkali cations and halide anions was determined by MD simulation at 298.15 K and low salinity (x_i= 0.001 mol/mol).

The simulation results of the self-diffusion coefficient of the investigated ions in ethanolic solution are shown in Figure 11 and listed in Table 8. An ion propagates together with its solvation shell through the electrolyte solution, and hence the ion motion is dominated by the effective radius of this ion-ethanol complex [6]. The formation of this complex is more pronounced the stronger the electrostatic interaction within the solvation shell [6]. In case of the alkali cations, the self-diffusion coefficient of Li$^+$ and Na$^+$, which have almost the same size, and the considerably larger K$^+$ are identical within their statistical simulation uncertain-

14

ties, cf. Figure 11 and Table 8. The underlying identical effective radius of the different ion-ethanol complexes can be attributed to the compensation of the influence of the decrease of the electrostatic attraction in the solvation shell by the increase of the ion diameter itself with increasing size of these cations. In case of the anions, a small increase of the self-diffusion coefficient with increasing size of the ions can be observed, cf. Figure 11 and Table 8. It is attributed to less pronounced ion-ethanol complexes due to decreasing electrostatic interaction between the anions and the ethanol molecules with increasing ion size. There is only a slight relative increase of the ion diameter from Cl^- to I^- and hence the influence of the ion diameter on the ion-ethanol complex around the anions is weak.

4.7. Electric conductivity

The electric conductivity σ of ethanolic sodium bromide and iodide salt solutions was determined at various concentrations at 298.15 K. These specific alkali halide salts were chosen because sufficient experimental data are available in the literature [59, 60].

The electric conductivity of the ethanolic NaBr and NaI salt solutions is shown in Figure 12. The predictions from molecular simulation follow the trend of the experiments [59], i.e. the changes of the absolute value of σ become smaller at higher concentrations. At low salinity, the electric conductivity of the ethanolic electrolyte solutions is well predicted by molecular simulation. With increasing concentration, an increasing mismatch between the simulation results of σ and the experimental data is observed. However, the deviations are throughout below the statistical uncertainties of the molecular simulation.

5. Conclusions

The density of all soluble ethanolic alkali halide salt solutions was determined at concentrations up to 0.05 mol/mol or 90 % of the solubility limit in a temperature range from 298.15 to 328.15 K at 1 bar both by experiment and molecular simulation. Furthermore, the radial distribution function of the ethanol sites around the ions, the solvation number and the residence time of ethanol molecules in the first solvation shell around the ions, the self-diffusion coefficient of the ions and the electric conductivity of ethanolic electrolyte solutions were determined by molecular simulation. The molecular force fields of the ions and ethanol were taken from previous work of our group and were not adjusted to properties of ethanolic alkali halide salt solutions.

The present experimental data of the density of ethanolic alkali halide salt solutions are in excellent agreement with data from the literature. Prior to this work, there was a lack of experimental density data both for LiBr and LiI solutions at 298.15 K. In case of the three other investigated temperatures, namely 308.15, 318.15 and 328.15 K, experimental density data of ethanolic alkali halide salt solutions were entirely missing in the literature. It is found that there is a linear relation between the density of the solution ρ and the ion mole fraction x_i. The predictions of the slopes a of that relation for the different salts and of the reduced density $\widetilde{\rho}$ of the solutions are in good agreement with the experimental data. There is almost no influence of the temperature on the reduced density and the slope a, which is well predicted by the molecular simulation. The prediction of these properties with ion force fields adjusted in aqueous solutions is feasible, as there is the same group of the solvent molecules in the same distance in the direct surrounding of the ions in both aqueous and ethanolic alkali halide solutions (primary effect).

16

Furthermore, the orientation of the ethanol molecules in the solvation shell around the ions (secondary effect) is predicted correctly by the molecular simulation.

In the RDF of the ethanol sites around the ions, the position of the first maximum $r_{\mathrm{max},1}$ for the hydroxyl group $g_{i-\mathrm{O}}(r)$ was found to be closer to both cations and anions than for the methylene $g_{i-\mathrm{CH2}}(r)$ and the methyl group $g_{i-\mathrm{CH3}}(r)$. A remarkable finding is the different order of the first maxima of $g_{i-\mathrm{CH2}}(r)$ and $g_{i-\mathrm{CH3}}(r)$ around cations and anions. The methylene group of the ethanol molecule is around cations closer to the ion than the methyl group, which is obverse around the anions. This change in the order of $r_{\mathrm{max},1}$ around the oppositely charged ions can be attributed to the angled shape of the ethanol molecule, the different orientation of the hydroxyl group around the ions and the interaction between the charge and the methylene group. Unfortunately, experimental data of the RDF of the ethanol sites around the alkali cations and halide anions are missing in the literature. It will be interesting to compare the present predictions to experimental data when such data will hopefully become available in the future.

The decline of the electrostatic interaction between the ion and the solvent is the reason for the decrease of the residence time $\tau_{i-\mathrm{O}}$ of ethanol molecules in the first solvation shell with increasing size of the cations. In case of the anions, where the electrostatic attraction between ions and surrounding ethanol molecules is weaker, $\tau_{i-\mathrm{O}}$ is only slightly longer than $\tau_{\mathrm{O}-\mathrm{O}}$ in pure liquid ethanol.

The increase of the self-diffusion coefficients D_i with increasing size of the ions can be attributed to the decreasing effective radius of the ion-ethanol complex, which typically dominates the mobility of the ion in the solution. However, with increasing size of the ion the effective radius of the ion-ethanol complex is increasingly influenced by the ion diameter itself. These opposing effects are the

17

reason for similar values for D_i in case of different alkali cations in ethanolic electrolyte solutions. The predictions from molecular simulation of the electric conductivity σ of ethanolic NaBr and NaI salt solutions are found to be in good agreement with experimental data from the literature.

The present study of ethanolic electrolyte solutions generalizes our previous work on aqueous and methanolic electrolyte solutions. They suggest that the present methodology should also yield good results for electrolyte solutions of alkali halide salts in other alcohols.

Appendix: Simulation details

All simulations of this study were carried out with the simulation program *ms*2 [57]. In *ms*2, thermophysical properties can be determined for rigid molecular models using Monte-Carlo (MC) or molecular dynamics (MD) simulation techniques. For all simulations, the LJ interaction partners are determined for every time step and MC loop, respectively. Interaction energies between molecules and/or ions are

determined explicitly for distances smaller than the cut-off radius r_c. The thermostat incorporated in *ms*2 is velocity scaling. The pressure is kept constant using Andersens barostat in MD, and random volume changes evaluated according to Metropolis acceptance criterion in MC, respectively. The simulation uncertainties were estimated with the block average method by Flyvberg and Petersen [61]. The liquid density of ethanolic alkali halide solutions was determined with the MC technique in the isothermal-isobaric (NpT) ensemble at a constant pressure of 1 bar for different temperatures and compositions. Depending on the composition, the simulation volume contained 2 to 50 cations. The molecule number in the simulations was set at least to $N = 1000$ and increased up to $N = 1111$. A physically reasonable configuration was obtained after 5000 equilibration loops in the canonical ensemble (NVT), followed by $80,000$ relaxation loops in the NpT ensemble. Thermodynamic averages were obtained by sampling $512,000$ loops. Each loop consisted of $N_{\mathrm{NDF}}/3$ steps, where N_{NDF} indicates the total number of mechanical degrees of freedom of the system. Electrostatic long range contributions were considered by Ewald summation [62] with a real space convergence parameter $\kappa = 5.6$. The real space cut-off radius was equal to the LJ cut-off radius of 21 Å.

For the calculation of structural and dynamic properties of the ethanolic electrolyte solutions, MD simulations were carried out. In a first step, the density of the ethanolic alkali halide solution was determined by an NpT simulation at the desired temperature, pressure and composition. Subsequently, the self-diffusion coefficient, the radial distribution function and the residence time were calculated in the NVT ensemble at the same temperature and composition with the density resulting from the first step. In these MD simulations, Newton's equations of mo-

tion were solved with a Gear predictor-corrector scheme of fifth order with a time step of 1.2 fs. The long-range interactions were considered by Ewald summation [62].

The self-diffusion coefficient of the ions [63] and the electric conductivity of the solution [64] were calculated with the Green-Kubo formalism [65, 66]. For simulations in the NpT ensemble, a physically reasonable configuration was attained by $10,000$ time steps in the NVT ensemble and $100,000$ time steps in the NpT ensemble, followed by a production run over $800,000$ time steps. In the NVT ensemble, the equilibration was carried out over $150,000$ time steps, followed by a production run of $6,000,000$ time steps for the calculation of the self-diffusion coefficient and the electric conductivity. The sampling length of the velocity and the electric current autocorrelation functions was set to 14 ps and the separation between the origins of two autocorrelation functions was 0.1 ps. Within this time span, all correlation functions decayed to less than 1/e of their normalized value. The MD unit cell with periodic boundary conditions contained 5000 molecules. This relative high number of molecules was used here to minimize the influence of the finite size effect on the simulation results. Using the Green-Kubo formalism [65, 66] for the calculation of transport properties of aqueous systems, Guevara-Carrion et al. [27] showed that the finite site effect saturates with increasing number of molecules. No significant differences were observed above 2048 molecules [27]. For the calculation of the self-diffusion coefficient, the simulation volume contained 4990 ethanol molecules, 5 alkali ions and 5 halide ions. The electric conductivity was determined for different compositions. Hence, the number of ions in the simulation volume varied from 7 to 145. The real space and LJ cut-off radius was set to 30 Å.

20

The radial distribution function and the residence time were determined by molecular simulation of systems containing 2 cations, 2 anions and 996 ethanol molecules. For simulations in the NpT ensemble, the system was equilibrated over $10,000$ time steps in the NVT ensemble and $100,000$ time steps in the NpT ensemble, followed by a production run over $2,000,000$ time steps. The resulting density was used in a subsequent NVT ensemble simulation for the determination of the RDF of ethanol around the ions. The RDF was sampled up to a cut-off radius of 21 Å with 704 bins. The results for the position of the first minimum of the RDF were used in a second NVT ensemble simulation with the same density for the determination of the residence time of ethanol molecules around the ions. In both NVT simulations, the system was equilibrated over $100,000$ time steps, followed by a production run of $1,000,000$ time steps.

The same process was applied for the calculation of the pure ethanol properties, i.e. the residence time of ethanol molecules around each other.
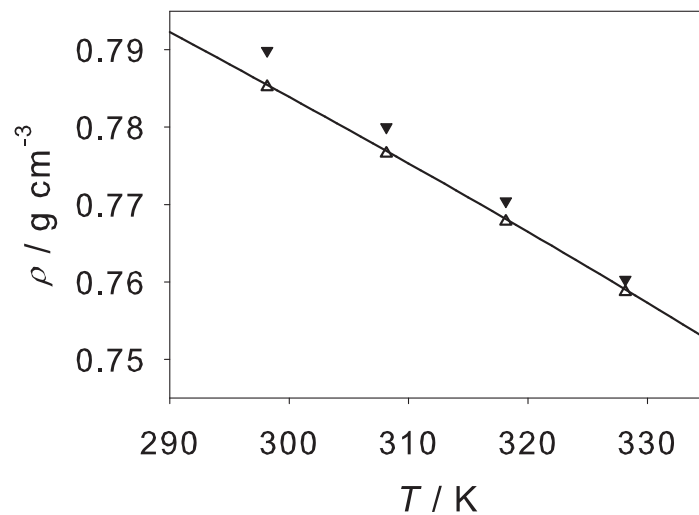
Figure 1: Density of pure liquid ethanol as a function of temperature at 1 bar. Simulation results from the present work (▼) are compared to present experimental data (△). The line indicates a correlation of experimental data from the literature [30].
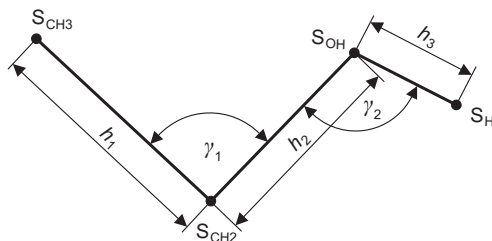
Figure 2: Geometry of the ethanol model by Schnabel et al. [25]: S_i indicates the model interaction site i.

22
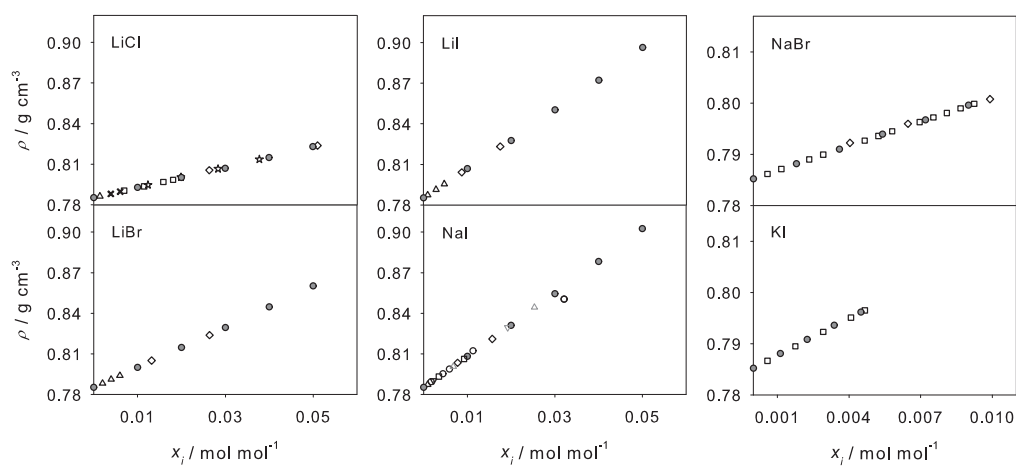
Figure 3: Density of ethanolic lithium chloride, lithium and sodium bromide and lithium, sodium and potassium iodide salt solutions as a function of the ion mole fraction at 298.15 K and 1 bar. Present experimental data (•) are compared to data from the literature: Kawaizumi and Zana [9](□), Vosburgh et al. [8](☆), Eliseeva et al. [11](×), Glugla et al. [10](△), Held et al. [12](◇), Taniewska-Osinska and Chadzynski [14](▽), Nowicka et al. [16](▽), Lauermann [15](△), Partington and Simpson [13](○).
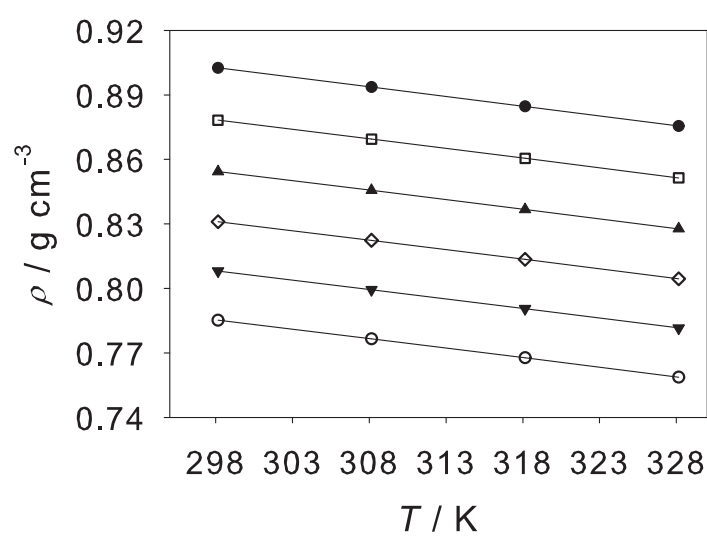
Figure 4: Density of pure ethanol (○) and ethanolic sodium iodide salt solutions as a function of temperature at ion mole fractions of x_i = 0.01 (▼), 0.02 (◇), 0.03 (▲), 0.04 (□) and 0.05 mol/mol (●) and 1 bar. The symbols represent the present experimental data and the lines are guides for the eye.
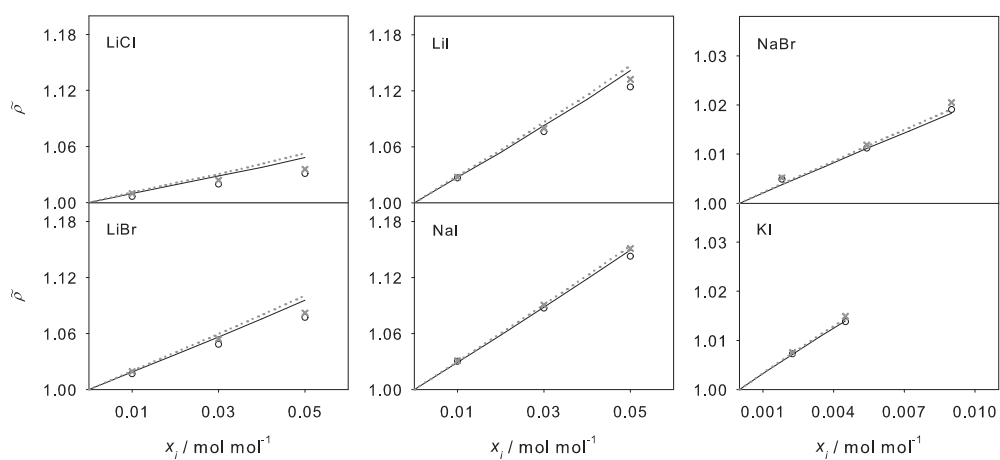
Figure 5: Reduced density of ethanolic lithium chloride, lithium and sodium bromide and lithium, sodium and potassium iodide salt solutions as a function of the ion mole fraction at 1 bar. Present simulation data (symbols) are compared to correlations of the present experimental data (lines): 298.15 K ($\circ$, —) and 328.15 K ($\times$, $\cdots$). For several solutions the lines and symbols of the different temperatures lie upon each other.
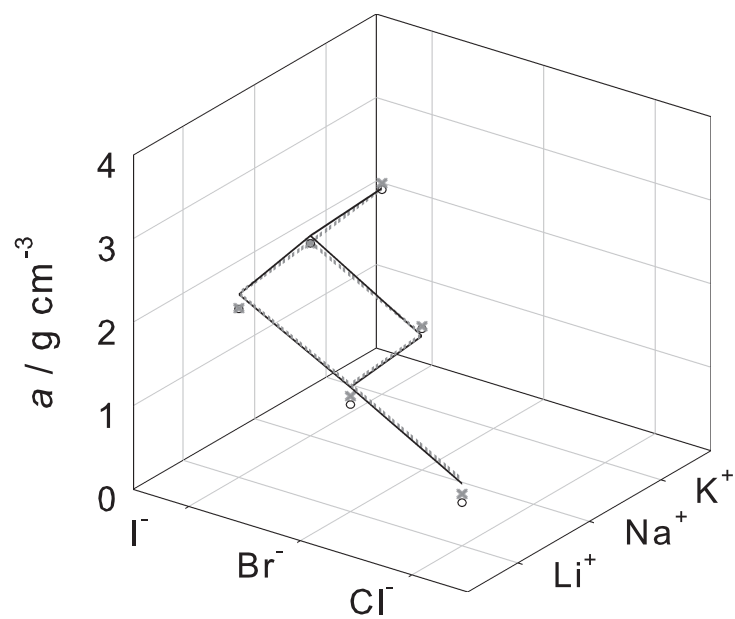
Figure 6: Slope of the density of ethanolic alkali halide salt solutions over the ion mole fraction (cf. Eq. 5) at 1 bar. Present simulation data (symbols) are compared to present experimental data (lines): 298.15 K ($\circ$, —) and 328.15 K ($\times$, $\cdots$). For several solutions the lines and symbols of the different temperatures lie upon each other.
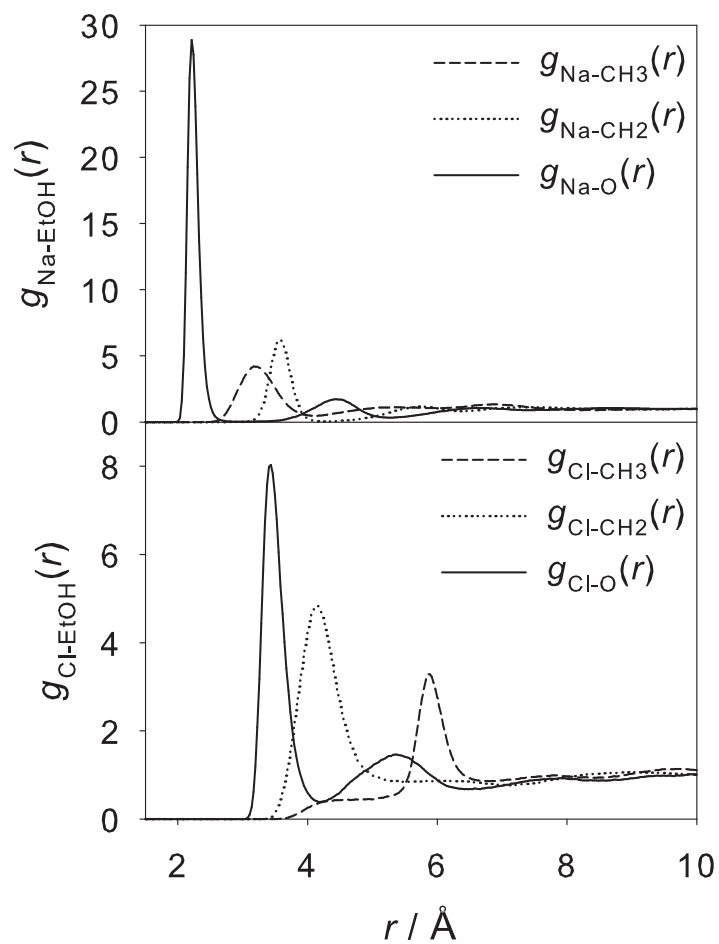
Figure 7: Radial distribution function of the oxygen atom (—), the methylene (· · ·) and the methyl group (- - -) of ethanol around Na$^+$ (top) and Cl$^-$ (bottom) in ethanolic solution (x_i=0.002 mol/mol) at 298.15 K and 1 bar. The LJ size parameters are σ_{Na}=1.89 Å, and σ_{Cl}=4.41 Å.
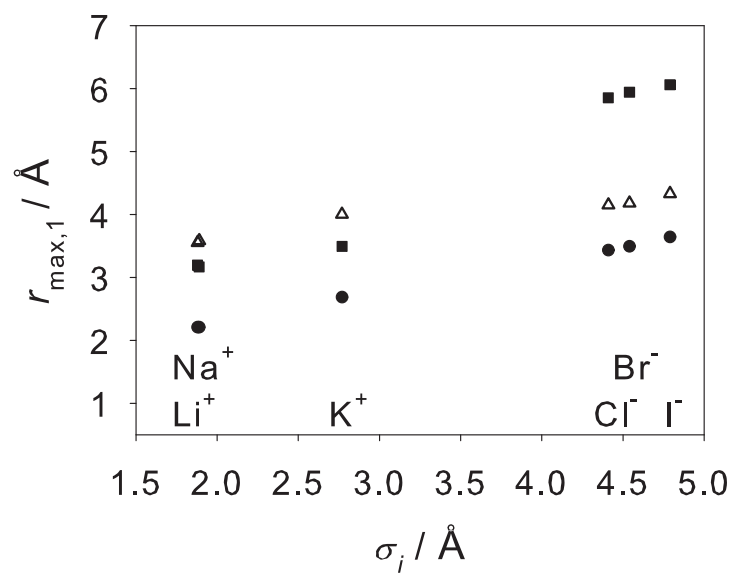
Figure 8: Position of the first maximum of the radial distribution function of the oxygen atom (•), the methylene (△) and the methyl group (■) of ethanol around the alkali cations and halide anions in ethanolic solution (x_i=0.002 mol/mol) at 298.15 K and 1 bar. For lithium and sodium, the LJ size parameters are almost identical and the simulation results are identical within their statistical uncertainties.
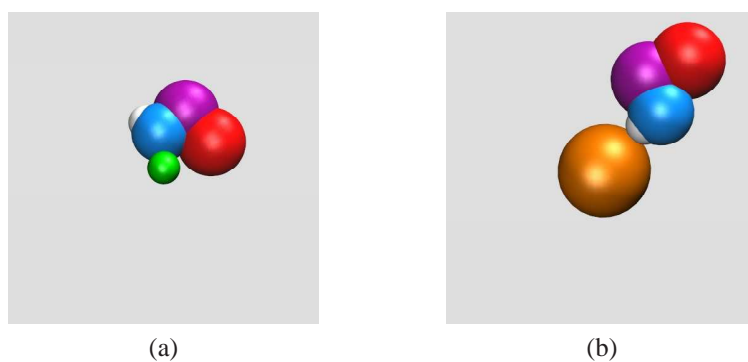
Figure 9: Screenshot of the molecular simulation of ethanolic NaCl salt solution at 298.15 K and 1 bar. All molecules are faded out except of one sodium cation (green) (a) and chloride anion (orange) (b), respectively, and one ethanol molecule of the corresponding solvation shell. The hydroxyl group of the ethanol molecule consists of the white hydrogen and the blue oxygen atom. The methylene and methyl group are represented by the purple and red sphere, respectively.
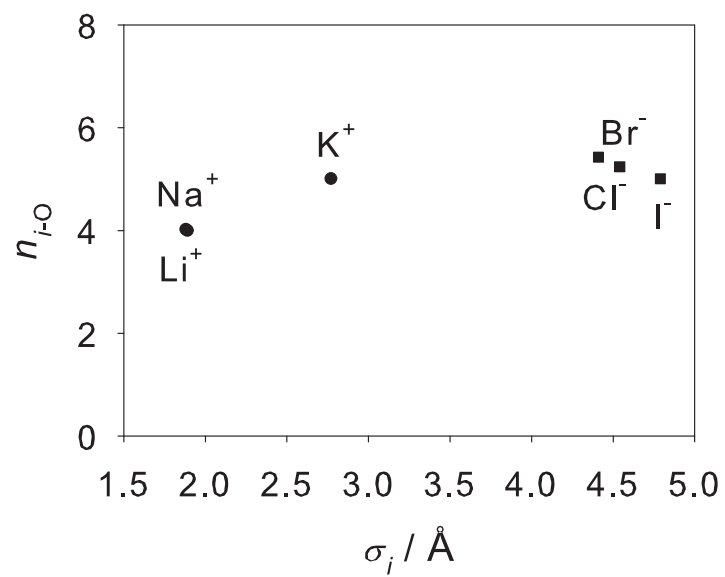
Figure 10: Solvation number of the first solvation shell around the alkali cations (•) and halide anions (■) in ethanolic solution (x_i=0.002 mol/mol) at 298.15 K and 1 bar. For lithium and sodium, the LJ size parameters and the simulation results are almost identical.
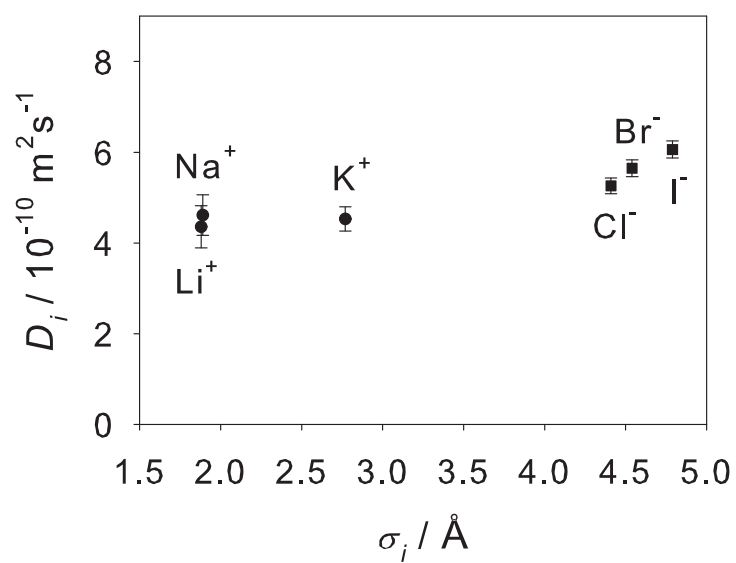
Figure 11: Self-diffusion coefficient of alkali cations (•) and halide anions (■) in ethanolic solutions (x_i = 0.001 mol/mol) at 298.15 K and 1 bar. For lithium and sodium, the LJ size parameters and the simulation results are almost identical.
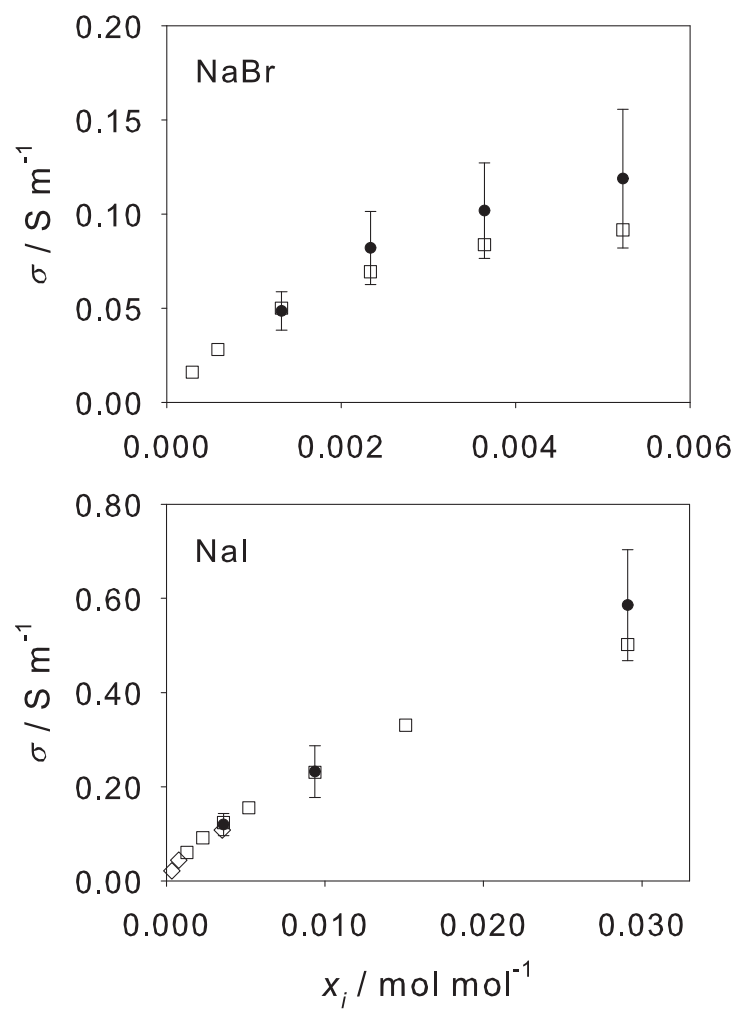
Figure 12: Electric conductivity of ethanolic sodium bromide and iodide salt solutions as a function of the ion mole fraction at 298.15 K and 1 bar. Present simulation data (●) are compared to experimental data from the literature: Nikitina et al. [59] (□) and Sukhotin and Timofeeva [60] (◇).

Table 1: Purity and supplier of the alkali halide salts.

salt	purity	supplier
LiCl	≥ 99 %	Merck
LiBr	≥ 99.999 %	Roth
LiI	≥ 99 %	AlfaAesar
NaBr	≥ 99 %	Merck
NaI	≥ 99.5 %	Roth
KI	≥ 99 %	Fluka

Table 2: LJ size parameter σ, LJ energy parameter ε, point charge and geometry parameters of the ethanol force field, cf. Figure 2. The parameters were taken from previous work [25].

Site	σ / Å	ε/k_B / K	q / e
S_{CH3}	3.6072	120.15	0
S_{CH2}	3.4612	80.291	+0.25560
S_{OH}	3.1496	85.053	-0.69711
S_H	0	0	+0.44151
	h_1 / Å	h_2 / Å	h_3 / Å
	1.98429	1.71581	0.95053
	γ_1 / °	γ_2 / °	
	90.950	106.368	

Table 3: LJ size parameter σ of alkali and halide ions. The LJ energy parameter ϵ/k_B is 200 K throughout. The parameters were taken from previous work [5, 6].

Ion	σ / Å
Li^+	1.88
Na^+	1.89
K^+	2.77
Rb^+	3.26
Cs^+	3.58
F^-	3.66
Cl^-	4.41
Br^-	4.54
I^-	4.78

Table 4: Experimental data of the density ρ of ethanolic alkali halide salt solutions and pure ethanol at 1 bar. The uncertainty in x_i is estimated to be better than ±0.00001 mol/mol. The uncertainty of the density and temperature measurements is found to be better than ±0.0001 g/cm^3 and ±0.1 K, respectively.

T / K		298.15	308.15	318.15	328.15
salt	x_i / mol mol^{-1}	ρ / g cm^{-3}			
LiCl	0.01000	0.7928	0.7844	0.7757	0.7669
	0.02000	0.8001	0.7918	0.7834	0.7747
	0.03000	0.8069	0.7987	0.7903	0.7818
	0.04000	0.8148	0.8067	0.7985	0.7902
	0.05000	0.8229	0.8150	0.8069	0.7986
LiBr	0.01000	0.8000	0.7915	0.7828	0.7739
	0.02000	0.8147	0.8063	0.7977	0.7889
	0.03000	0.8294	0.8211	0.8126	0.8039
	0.04000	0.8447	0.8364	0.8280	0.8194
	0.05000	0.8602	0.8520	0.8437	0.8352
LiI	0.01000	0.8068	0.7982	0.7895	0.7806
	0.02000	0.8276	0.8191	0.8104	0.8015
	0.03000	0.8502	0.8417	0.8330	0.8242
	0.04000	0.8721	0.8636	0.8550	0.8462
	0.05000	0.8963	0.8879	0.8792	0.8704
NaBr	0.00180	0.7882	0.7796	0.7708	0.7618
	0.00360	0.7910	0.7824	0.7736	0.7646
	0.00540	0.7939	0.7853	0.7765	0.7676
	0.00720	0.7967	0.7881	0.7794	0.7704
	0.00900	0.7996	0.7910	0.7823	0.7733
NaI	0.01000	0.8081	0.7994	0.7906	0.7816
	0.02000	0.8310	0.8224	0.8135	0.8045
	0.03000	0.8544	0.8457	0.8368	0.8277
	0.04000	0.8782	0.8694	0.8605	0.8514
	0.05000	0.9025	0.8937	0.8847	0.8755
KI	0.00113	0.7881	0.7795	0.7707	0.7616
	0.00225	0.7908	0.7822	0.7734	0.7644
	0.00338	0.7936	0.7850	0.7762	0.7671
	0.00450	0.7962	0.7875	0.7787	0.7697
EtOH		0.7852	0.7766	0.7678	0.7587

Table 5: Slope a of the density ρ of ethanolic alkali halide salt solutions over the ion mole fraction x_i at 1 bar. The standard deviation $\Delta\rho$ of the correlation for the density of ethanolic electrolyte solutions (Eq. (5)) is for all studied alkali halide salts below ± 0.001 g/cm^3.

T / K	298.15	328.15		298.15	328.15		298.15	328.15
Salt	a / g cm^{-3}		Salt	a / g cm^{-3}		Salt	a / g cm^{-3}	
LiCl	0.74	0.79						
LiBr	1.49	1.52	NaBr	1.60	1.62			
LiI	2.19	2.20	NaI	2.33	2.32	KI	2.47	2.47

Table 6: Molecular simulation data of the density ρ of ethanolic alkali halide salt solutions and pure ethanol at 1 bar. The statistical uncertainties of the densities are throughout below ± 0.0003 g/cm^3.

T / K		298.15	308.15	318.15	328.15
salt	x_i / mol mol^{-1}	ρ / g cm^{-3}			
LiCl	0.01000	0.7950	0.7867	0.7766	0.7677
	0.03000	0.8054	0.7972	0.7877	0.7785
	0.05000	0.8144	0.8048	0.7950	0.7875
LiBr	0.01000	0.8032	0.7940	0.7845	0.7750
	0.03000	0.8281	0.8197	0.8120	0.8015
	0.05000	0.8510	0.8430	0.8319	0.8227
LiI	0.01000	0.8109	0.8019	0.7922	0.7812
	0.03000	0.8501	0.8404	0.8292	0.8209
	0.05000	0.8879	0.8809	0.8708	0.8609
NaBr	0.00180	0.7938	0.7843	0.7736	0.7642
	0.00540	0.7987	0.7893	0.7793	0.7693
	0.00900	0.8050	0.7961	0.7867	0.7759
NaI	0.01000	0.8137	0.8047	0.7949	0.7839
	0.03000	0.8587	0.8489	0.8377	0.8292
	0.05000	0.9027	0.8956	0.8853	0.8752
KI	0.00225	0.7956	0.7856	0.7762	0.7661
	0.00450	0.8008	0.7920	0.7818	0.7716
EtOH		0.7899	0.7800	0.7705	0.7603

Table 7: RDF of the oxygen atom $g_{i-\mathrm{O}}(r)$, the methylene $g_{i-\mathrm{CH2}}(r)$ and the methyl group $g_{i-\mathrm{CH3}}(r)$ of ethanol around the alkali and halide ions i in ethanolic solutions (x_i =0.002 mol/mol) at the first maximum $r_{\mathrm{max,1}}$, first minimum $r_{\mathrm{min,1}}$ and second maximum $r_{\mathrm{max,2}}$ at 1 bar.

| | $r_{\mathrm{max,1}}$ / Å | | | $g(r_{\mathrm{max,1}})$ | | |
Ion	i-O	i-CH2	i-CH3	i-O	i-CH2	i-CH3
Li$^+$	2.211	3.555	3.196	28.569	6.342	4.303
Na$^+$	2.211	3.585	3.166	28.866	6.231	4.199
K$^+$	2.688	4.003	3.495	16.406	4.662	3.582
Cl$^-$	3.435	4.152	5.855	8.033	4.845	3.287
Br$^-$	3.495	4.182	5.945	7.233	4.644	3.116
I$^-$	3.644	4.331	6.064	6.185	4.272	2.854
	$r_{\mathrm{min,1}}$ / Å			$g(r_{\mathrm{min,1}})$		
Ion	i-O	i-CH2	i-CH3	i-O	i-CH2	i-CH3
Li$^+$	2.987	4.272	4.092	0.016	0.050	0.448
Na$^+$	2.957	4.272	4.092	0.019	0.049	0.466
K$^+$	3.585	4.809	4.750	0.110	0.199	0.626
Cl$^-$	4.182	5.676	6.811	0.391	0.842	0.856
Br$^-$	4.272	5.526	6.811	0.404	0.811	0.815
I$^-$	4.421	5.825	7.050	0.447	0.784	0.820
	$r_{\mathrm{max,2}}$ / Å			$g(r_{\mathrm{max,2}})$		
Ion	i-O	i-CH2	i-CH3	i-O	i-CH2	i-CH3
Li$^+$	4.451	5.765	6.871	1.852	1.188	1.323
Na$^+$	4.421	5.765	6.871	1.725	1.180	1.336
K$^+$	4.809	6.124	7.319	1.317	1.027	1.302
Cl$^-$	5.377	6.064	7.826	1.463	0.880	0.995
Br$^-$	5.317	6.303	8.006	1.433	0.866	0.977
I$^-$	5.437	6.572	8.125	1.478	0.846	0.964

Table 8: Solvation number $n_{i-\mathrm{O}}$ and residence time $\tau_{i-\mathrm{O}}$ of ethanol molecules in the first solvation shell around the alkali and halide ions i in ethanolic solutions (x_i = 0.002 mol/mol) and their self-diffusion coefficient D_i in ethanolic solutions (x_i = 0.001 mol/mol) at 298.15 K and 1 bar. The number in parentheses indicates the statistical simulation uncertainty in the last digit.

Ion	$n_{i-\mathrm{O}}$	$\tau_{i-\mathrm{O}}$ / ps	D_i / 10^{-10} m^{2}s^{-1}
Li$^+$	4.0 (2)	91 (5)	4.3 (5)
Na$^+$	4.0 (2)	72 (3)	4.6 (4)
K$^+$	5.0 (2)	14 (1)	4.5 (3)
Cl$^-$	5.4 (2)	2.7 (2)	5.3 (2)
Br$^-$	5.2 (2)	4.3 (3)	5.5 (2)
I$^-$	5.0 (2)	2.8 (2)	6.1 (2)

[1] J. Barthel, H. J. Gores, G. Schmeer, R. Wachter, Non-Aqueous Electrolyte-Solutions in Chemistry and Modern Technology, Topics in Current Chemistry 111 (1983) 33–144.

[2] H. J. Gores, J. Barthel, Non-Aqueous Eletrolyte-Solutions - Promising Materials for Electrochemical Technologies, Naturwissenschaften 70 (1983) 495–503.

[3] J. Barthel, H. Krienke, W. Kunz, Physical Chemistry of Electrolyte Solutions, Springer, 1998.

[4] S. Reiser, M. Horsch, H. Hasse, Density of Methanolic Alkali Halide Salt Solutions by Experiment and Molecular Simulation, Journal of Chemcial & Engineering Data (2015) *accepted*.

[5] S. Deublein, J. Vrabec, H. Hasse, A set of molecular models for alkali and halide ions in aqueous solution, The Journal of Chemical Physics 136 (2012) 084501.

[6] S. Reiser, S. Deublein, J. Vrabec, H. Hasse, Molecular dispersion energy parameters for alkali and halide ions in aqueous solution, The Journal of Chemical Physics 140 (2014) 044504.

[7] T. Schnabel, A. Srivastava, J. Vrabec, H. Hasse, Hydrogen bonding of methanol in supercritical CO_2: Comparison between ^{1}H NMR spectroscopic data and molecular simulation results, Journal of Physical Chemistry B 111 (2007) 9871–9878.

[8] W. C. Vosburgh, L. C. Connell, J. A. V. Butler, The Electrostriction Produced

by Salts in some Aliphatic Alcohols, Journal of the Chemical Society (1933) 933–942.

[9] F. Kawaizumi, R. Zana, Partial Molal Volumes of Ions in Organic Solvents from Ultrasonic Vibration Potential and Density Measurements. 2. Ethanol and Dimethylformamide, Journal of Physical Chemistry 78 (1974) 1099–1105.

[10] P. G. Glugla, J. H. Byon, C. A. Eckert, Partial Molar Volume of Some Monovalent Salts and Polar Molecules in Organic Solvents, Journal of Chemical & Engineering Data 27 (1982) 393–398.

[11] O. V. Eliseeva, V. V. Golubev, A. A. Dyshin, M. G. Kiselev, G. A. Al'per, A volumetric investigation of solvophobic effects in halide-n-alkanol-n-alkane ternary systems, Russian Journal of Physical Chemistry 80 (2006) 205–209.

[12] C. Held, A. Prinz, V. Wallmeyer, G. Sadowski, Measuring and Modeling Alcohol/Salt Systems, Chemical Engineering Science 68 (2012) 328–339.

[13] J. R. Partington, H. G. Simpson, Concentration Cells in Ethyl Alcohol. Part V. Cells Without Liquid Junctions, Transactions of the Faraday Society 26 (1930) 625–634.

[14] S. Taniewska-Osinska, P. Chadzynski, Viscosity of NaI Solutions in Mixtures of Water with Methanol, Ethanol and n-Propanol, Acta Universitatis Lodziensis 6 (1976) 37–46.

[15] G. Lauermann, Dampfdruckuntersuchungen an Lösungen von Natriumjodid in Ethanol und iso-Propanol, Ph.D. thesis, University of Regensburg (1982).

[16] B. Nowicka, A. Kacperska, J. Barczynska, A. Bald, S. Taniewska-Osinska, Viscosity of Solutions of NaI and $CaCl_2$ in Water-Ethanol and of NaI in Water-Tetrahydrofuran Mixtures, Journal of the Chemical Society - Faraday Transactions I 84 (1988) 3877–3884.

[17] H. Yan, S. Murad, E. Enciso, Molecular simulation of membrane based separations of ethanolic electrolyte solutions, Fluid Phase Equilibria 183 (2001) 279–287.

[18] Y. Zeng, J. Hu, Y. Yuan, X. Zhang, S. Ju, Car-Parrinello molecular dynamics simulations of Na^+ solvation in water, methanol and ethanol, Chemical Physics Letters 538 (2012) 60–66.

[19] Y. Zeng, C. Wang, X. Zhang, S. Ju, Solvation structure and dynamics of Li^+ ion in liquid water, methanol and ethanol: A comparison study, Chemical Physics 433 (2014) 89–97.

[20] W. L. Jorgensen, Optimized Intermolecular Potential Functions for Liquid Alcohols, Journal of Physical Chemistry 90 (1986) 1276–1284.

[21] W. L. Jorgensen, B. Bigot, J. Chandrasekhar, Quantum and Statistical Mechanical Studies of Liquids. 21. Nature of Dilute-Solutions of Sodium and Methoxide Ions in Methanol, Journal of the American Chemical Society 104 (1982) 4584–4591.

[22] W. Jorgensen, D. Maxwell, J. Tirado-Rives, Development and testing of the OPLS all-atom force field on conformational energetics and properties of organic liquids, Journal of the American Chemical Society 118 (1996) 11225–11236.

[23] B. Chen, J. Potoff, J. Siepmann, Monte Carlo calculations for alcohols and their mixtures with alkanes. Transferable potentials for phase equilibria. 5. United-atom description of primary, secondary, and tertiary alcohols, Journal of Physical Chemistry B 105 (15) (2001) 3093–3104.

[24] R. Taylor, R. Shields, Molecular-dynamics simulations of the ethanol liquid-vapor interface, The Journal of Chemical Physics 119 (2003) 12569–12576.

[25] T. Schnabel, J. Vrabec, H. Hasse, Henry's law constants of methane, nitrogen, oxygen and carbon dioxide in ethanol from 273 to 498 K: Prediction from molecular simulation, Fluid Phase Equilibria 233 (2005) 134–143.

[26] G. Guevara-Carrion, C. Nieto-Draghi, J. Vrabec, H. Hasse, Prediction of Transport Properties by Molecular Simulation: Methanol and Ethanol and Their Mixture, Journal of Physical Chemistry B 112 (2008) 16664–16674.

[27] G. Guevara-Carrion, J. Vrabec, H. Hasse, Prediction of self-diffusion coefficient and shear viscosity of water and its binary mixtures with methanol and ethanol by molecular simulation, The Journal of Chemical Physics 134 (2011) 074508.

[28] S. Reiser, N. McCann, M. Horsch, H. Hasse, Hydrogen Bonding of Ethanol in Supercritical Mixtures with CO_2 by ^{1}H NMR Spectroscopy and Molecular Simulation, Journal of Supercritical Fluids 68 (2012) 94–103.

[29] S. Parez, G. Guevara-Carrion, H. Hasse, J. Vrabec, Mutual diffusion in the ternary mixture of water plus methanol plus ethanol and its binary subsystems, Physical Chemistry Chemical Physics 15 (2013) 3985–4001.

[30] H. E. Dillon, S. G. Penoncello, A Fundamental Equation for Calculation of the Thermodynamic Properties of Ethanol, International Journal of Thermophysics 25 (2004) 321–335.

[31] H. J. C. Berendsen, J. R. Grigera, T. P. Straatsma, The Missing Term In Effective Pair Potentials, Journal of Physical Chemistry 91 (1987) 6269–6271.

[32] S. Reiser, M. Horsch, H. Hasse, Temperature Dependence of the Density of Aqueous Alkali Halide Salt Solutions by Experiment and Molecular Simulation, Journal of Chemical & Engineering Data 59 (2014) 3434–3448.

[33] H. E. Patten, W. R. Mott, Decomposition curves of lithium chloride in alcohols, and the electrodeposition of lithium, Journal of Physical Chemistry 8 (1904) 153–195.

[34] W. Turner, C. Bissett, The solubilities of alkali haloids in methyl, ethyl, propyl, and isoamyl alcohols, Journal of the Chemical Society 103 (1913) 1904–1910.

[35] W. P. Baxter, The inter-ionic attraction theory of ionized solutes. V. Testing of the theory by solubility experiments at higher temperatures, Journal of the American Chemical Society 48 (1926) 615–621.

[36] F. E. King, J. R. Partington, The solubility of sodium iodide in ethyl alcohol, Journal of the Chemical Society 128 (1926) 20–22.

[37] D. G. R. Bonnell, W. J. Jones, The equilibrium between ethyl alcohol and the alkali and alkaline-earth salts. Part I., Journal of the Chemical Society (1926) 318–321.

[38] F. G. Germuth, The solubilities of alkali bromides and fluorides in anhydrous methanol, ethanol, and butanol, Journal of the Franklin Institute 212 (1931) 343–349.

[39] G. Ferner, M. Mellon, Analytical uses of 2-Propanol, Industrial & Engineering Chemistry Analytical Edition 6 (1934) 345–348.

[40] J. P. Simmons, H. Freimuth, H. Russell, The systems lithium chloride-water-ethyl alcohol and lithium bromide-water-ethyl alcohol, Journal of the American Chemical Society 58 (1936) 1692–1695.

[41] R. G. Larson, H. Hunt, Molecular forces and solvent power, Journal of Physical Chemistry 43 (1939) 417–423.

[42] N. A. Izmailov, V. S. Chernyi, Thermodynamic Properties of Electrolytes in Non-Aqueous Solutions. VII. Investigation of the Solubility of Silver Chloride and Cesium Chloride in Alcohols, Ketones, and Mixed Solvents by Means of Radioactive Tracers, Russian Journal of Physical Chemistry 34 (1960) 58–61.

[43] I. P. Nikitina, B. S. Krumgalz, D. G. Traber, G. F. Fedotova, The Solubility of Potassium Salts in Ethanol, Russian Journal of Inorganic Chemistry 14 (1969) 2593–2594.

[44] G. Delesall, J. Heubel, Relation Between Solubility of Electrolytes and Dielectric-Constant of Solution, in Mixed Water-Ethanol Solvents at 25 C, Bulletin de la Societe Chimique de France (1972) 2626–2631.

[45] Y. G. Vlasov, P. P. Antonov, V. N. Anokhin, System LiCl-LiBr-C_2H_5OH at 25 C, Journal of Applied Chemistry of the USSR 48 (1975) 1207–1208.

[46] V. E. Plyushchev, I. V. Shakhno, L. N. Komissarova, G. V. Nadezhdina, Study of Solubility of Alkali Metal Chlorides in some Aliphatic Alcohols, Transactions of the Moscow Chemical-Technology Institute 7 (1985) 45 – 58.

[47] N. V. Kulikova, B. A. Kulikov, Solubility of Cesium-Crystals in Aliphatic Alcohol, Russian Journal of Inorganic Chemistry 33 (1988) 2968–2969.

[48] S. P. Pinho, E. A. Macedo, Representation of salt solubility in mixed solvents: A comparison of thermodynamic models, Fluid Phase Equilibria 116 (1996) 209–216.

[49] A. K. S. Labban, Y. Marcus, The solubility and solvation of salts in mixed nonaqueous solvents. 2. Potassium halides in mixed protic solvents, Journal of Solution Chemistry 26 (1997) 1–12.

[50] W.-X. Zhao, M.-C. Hu, Y.-C. Jiang, S.-N. Li, Solubilities, densities and refractive indices of rubidium chloride or cesium chloride in ethanol aqueous solutions at different temperatures, Chinese Journal of Chemistry 25 (2007) 478–483.

[51] R. R. Pawar, S. B. Nahire, M. Hasan, Solubility and Density of Potassium Iodide in Binary Ethanol-Water Solvent Mixture at 298.15, 303.15, 308.15, and 313.15 K, Journal of Chemical & Engineering Data 54 (2009) 1935 – 1937.

[52] M. Li, D. Constantinescu, L. Wang, A. Mohs, J. Gmehling, Solubilities of NaCl, KCl, LiCl, and LiBr in Methanol, Ethanol, Acetone, and Mixed Sol-

vents and Correlation Using the LIQUAC Model, Industrial & Engineering Chemistry Research 49 (2010) 4981–4988.

[53] R. R. Pawar, C. S. Aher, J. D. Pagar, S. L. Nikam, M. Hasan, Solubility, Density and Solution Thermodynamics of NaI in Different Pure Solvents and Binary Mixtures, Journal of Chemcial & Engineering Data 57 (2012) 3563–3572.

[54] H. A. Lorentz, Über die Anwendung des Satzes vom Virial in der kinetischen Theorie der Gase, Annalen der Physik 248 (1881) 127–136.

[55] D. Berthelot, Sur le melange des gaz, Comptes Rendus de l'Academie des Sciences 126 (1898) 1703–1706.

[56] R. W. Impey, P. A. Madden, I. R. McDonald, Hydration And Mobility of Ions in Solution, Journal of Physical Chemistry 87 (1983) 5071–5083.

[57] C. W. Glass, S. Reiser, G. Rutkai, S. Deublein, A. Köster, A. Guevara-Carrion, G. Wafai, M. Horsch, M. Bernreuther, T. Windmann, H. Hasse, J. Vrabec, *ms*2: A molecular simulation tool for thermodynamic properties, new version release, Computer Physics Communications 185 (2014) 3302–3306.

[58] S. Chowdhuri, A. Chandra, Solute size effects on the solvation structure and diffusion of ions in liquid methanol under normal and cold condition, The Journal of Chemical Physics 124 (2006) 084507.

[59] I. P. Nikitina, B. S. Krumgalz, D. G. Traber, Electrical Conductivity of Non-aqueous Electrolyte Solutions. I. Solutions of Sodium Salts in Ethyl Alcohol

in the Temperature Range from -60 to 60 C, Russian Journal of Electrochemistry 8 (1972) 629–630.

[60] A. M. Sukhotin, Z. N. Timofeeva, Association of Ions in Solutions. 2. The Causes of Anomalous Electroconductivity, Russian Journal of Physical Chemistry 33 (1959) 1602–1609.

[61] H. Flyvbjerg, H. G. Petersen, Error-Estimates On Averages of Correlated Data, The Journal of Chemical Physics 91 (1989) 461–466.

[62] P. P. Ewald, Die Berechnung optischer und elektrostatischer Gitterpotenziale, Annalen der Physik 369 (1921) 253–287.

[63] K. Gubbins, Statistical Mechanics Vol. 1, The Chemical Society Burlington House, London, 1972.

[64] J. P. Hansen, I. McDonald, Theory of Simple Liquids, Academic Press, Amsterdam, 1986.

[65] M. Green, Markoff Random Processes and the Statistical Mechanics of Time-Dependent Phenomena. 2. Irreversible Processes in Fluids, The Journal of Chemical Physics 22 (1954) 398–413.

[66] R. Kubo, Statistical-Mechanical Theory of Irreversible Processes. 1. General Theory and Simple Applications to Magnetic and Conduction Problems, Journal of the Physical Society of Japan 12 (1957) 570–586.